Supplemental information

Prolyl endopeptidase-like is a (thio)esterase

involved in mitochondrial respiratory chain function

Karen Rosier, Molly T. McDevitt, Joél Smet, Brendan J. Floyd, Maxime Verschoore, Maria J. Marcaida, Craig A. Bingman, Irma Lemmens, Matteo Dal Peraro, Jan Tavernier, Benjamin F. Cravatt, Natalia V. Gounko, Katlijn Vints, Yenthe Monnens, Kritika Bhalla, Laetitia Aerts, Edrees H. Rashan, Arnaud V. Vanlander, Rudy Van Coster, Luc Régal, David J. Pagliarini, and John W.M. Creemers
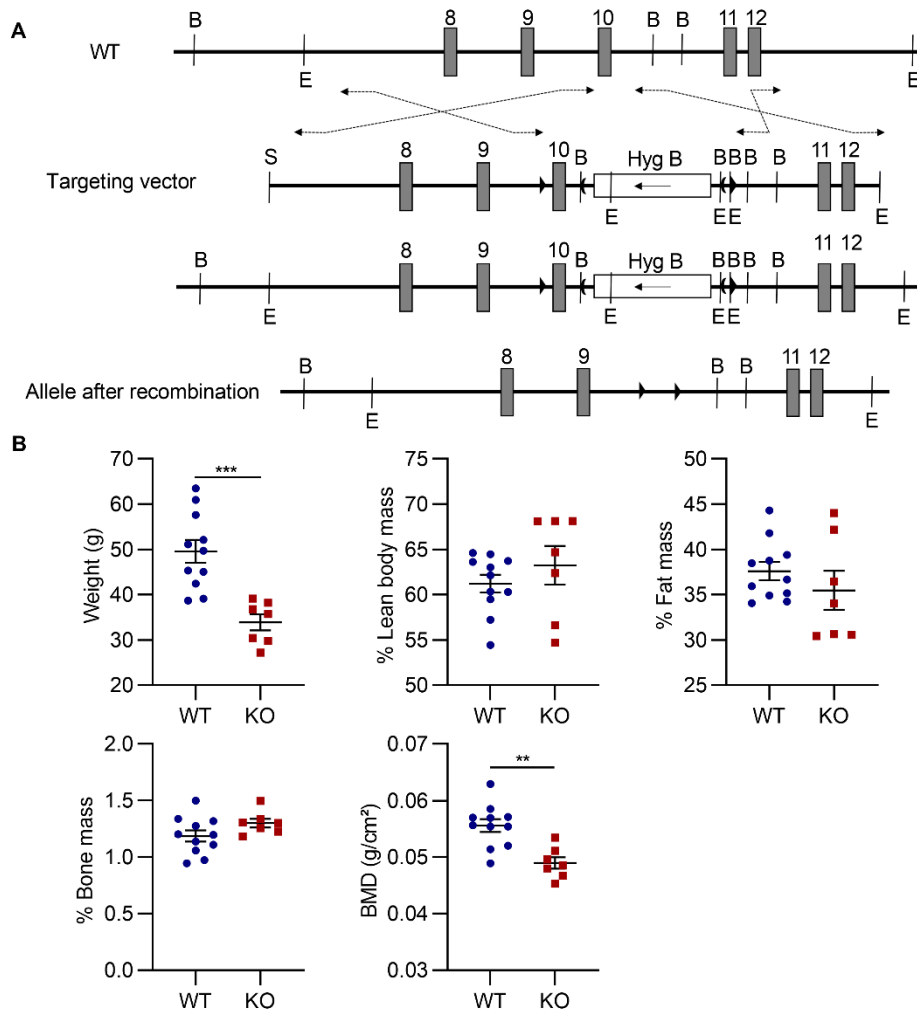
Figure S1. Generation and characterization of *Prepl* KO mouse model. Related to Figure 1. A. A targeting vector was designed for homologous recombination in embryonic stem cells (ES). Exon 10 of *Prepl* was cloned between two LoxP sites (triangle). A hygromycin B selection cassette (Hyg B), flanked by Frt sites (moon), was inserted downstream of exon 10. ES targeted cells were injected in blastocysts to generate chimeric mice, which were backcrossed either 1x or 8x to C57BL/6. Restriction sites used for cloning and Southern blot analysis are abbreviated as S (SalI), B (BglI) and E (EcoRI). B. Scatter plots of DEXA scan analysis in 9-month-old male mice reveals significant differences in bone mineral density (BMD) of *Prepl* WT and KO mice (n=7-11). Data represented as mean ± SEM; Unpaired Student's t-test; ** p<0.01, *** p<0.001. There were no significant differences in bone mass, lean body mass or fat mass relative to total scanned body mass between WT and KO mice. No significant differences between WT mice and heterozygous mice were found (data not shown).
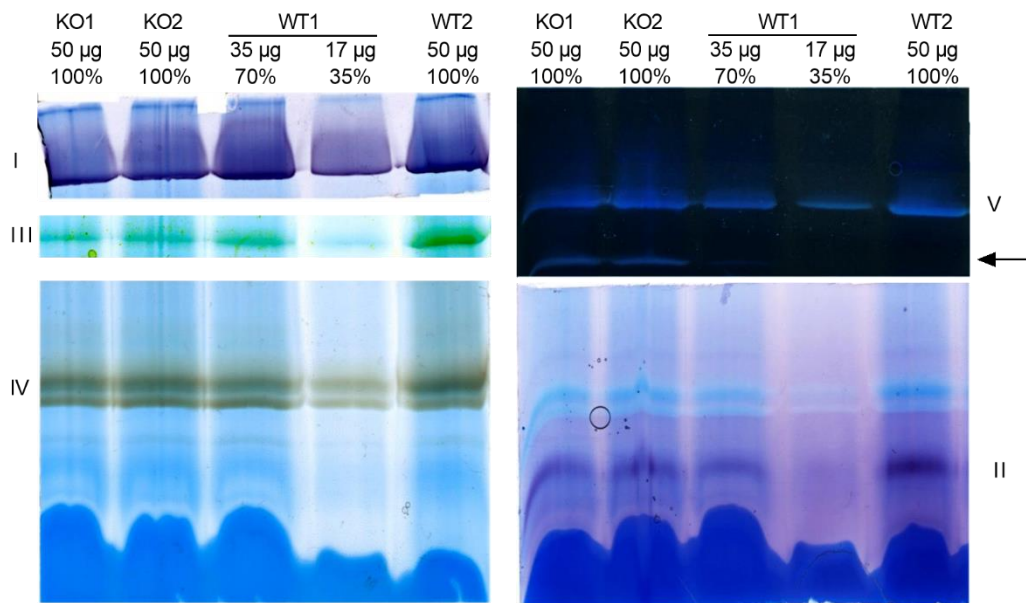
Figure S2. BN-PAGE reveals complex V subcomplexes in quadriceps of *Prepl* KO mice. Related to Figure 3. BN-PAGE followed by in-gel activity staining show decreased complex I, III and IV activity. The activity of these complexes in *Prepl KO* mice is similar to 70% of the activity of the complexes in WT controls, consistent with the 30% reduction observed in the spectrophotometric analysis. In addition, subcomplexes of complex V (arrow) are observed in KO samples, suggesting defective mitochondrial protein translation.
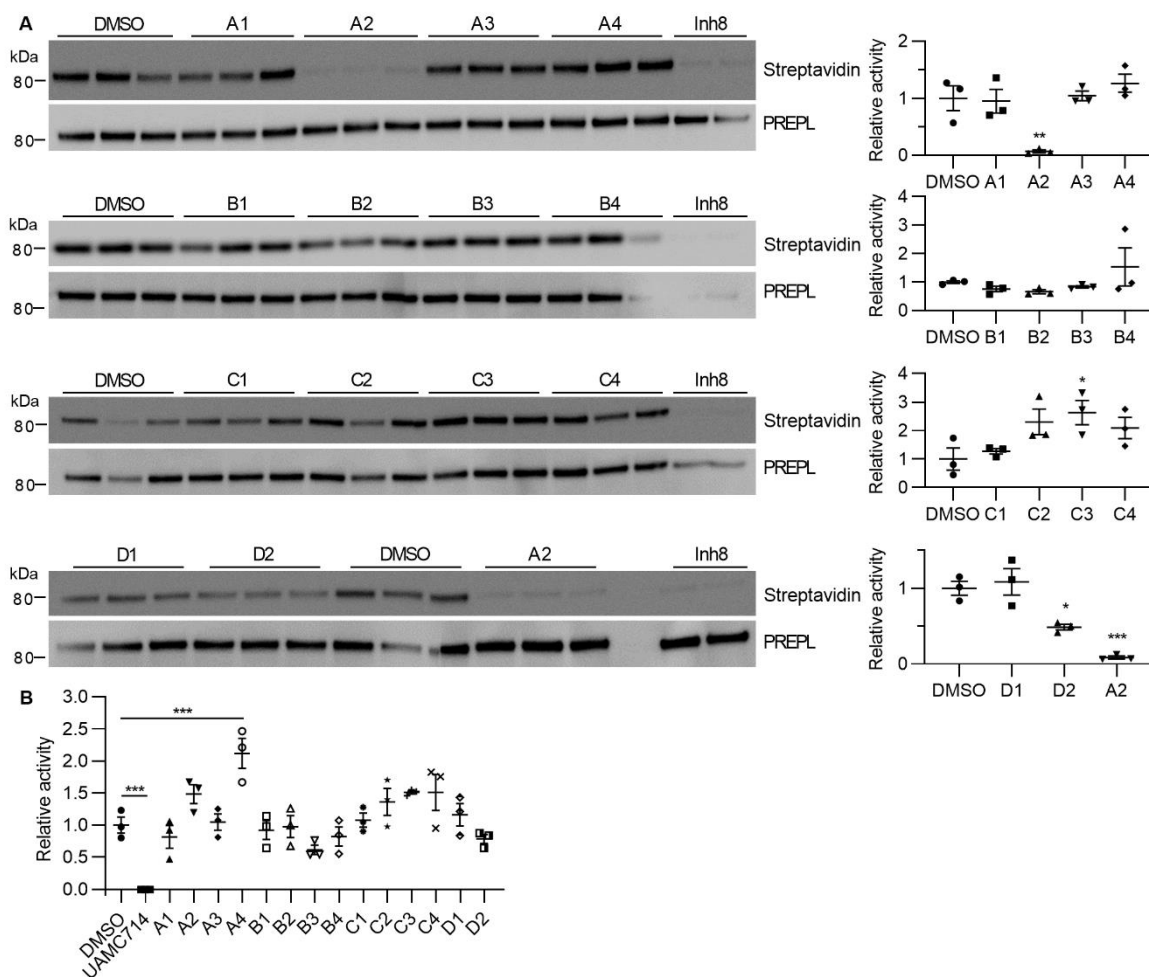
Figure S3. Inhibitor profile of PREPL and PREP. Related to Figure 4.
A. Competition experiment between serine hydrolase inhibitors and the activity-based probe FP-biotin. Interaction with FP-biotin is reduced when PREPL is incubated with Palmostatin M (A2) and WHP313 (D2). Streptavidin blots show the activity of PREPL with the activity-based probe. Blots labeled with GST antibody are the loading control of PREPL. Chemical structures of the inhibitors are collected in Table S4. B. Inhibitor profile of PREP. The serine hydrolase inhibitors from panel A were screened in an AMC substrate-based activity assay. Hydrolysis of the AMC substrate in the presence of DMSO was used as negative control. KYP-2047 (UAMC714) is a potent inhibitor of PREP. A-B. Data are presented as mean ± SEM (n=3); differences to DMSO control were analyzed by one-way ANOVA with Dunnett's multiple comparison test; * p<0.05, ** p<0.01; *** p<0.001.
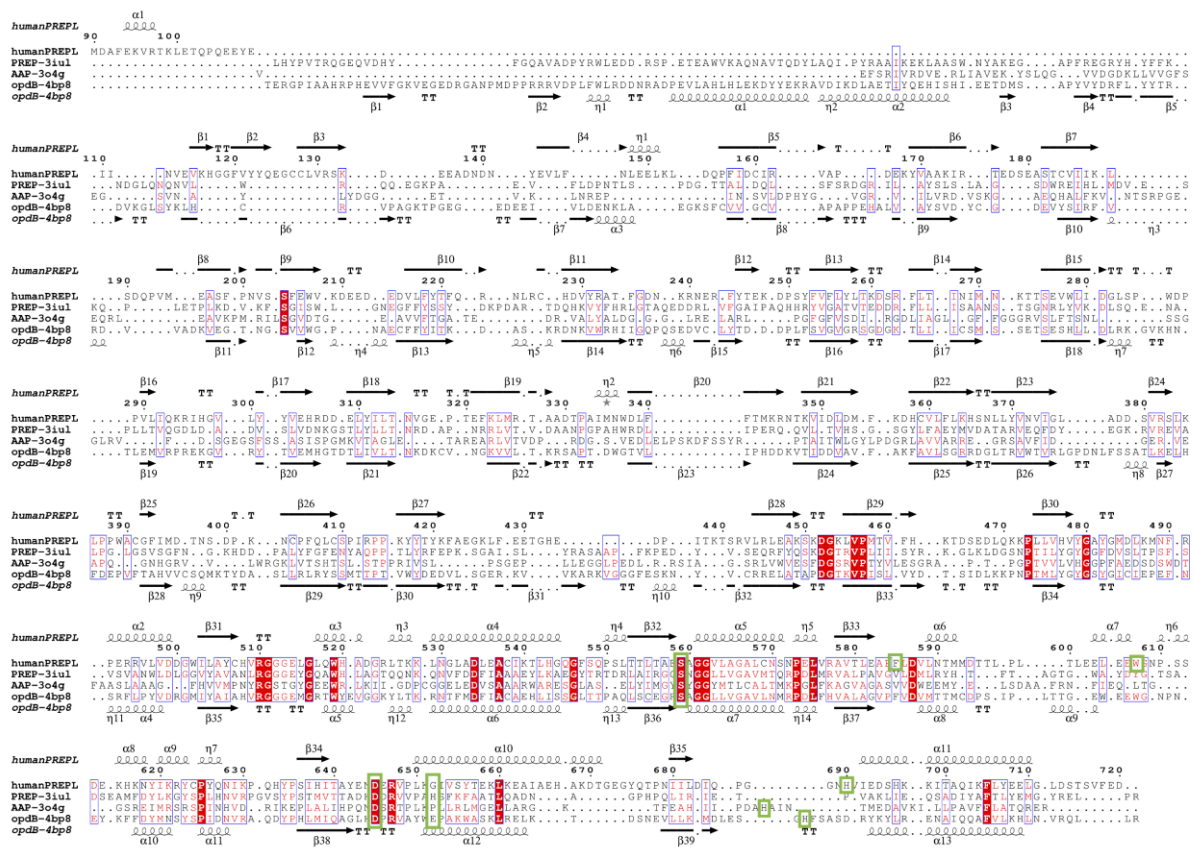
Figure S4. Structure-based sequence alignment of PREPL_S, PREP, OpdB and AAP. Related to Figure 5.

The inactive open structures of PREP, OpdB and AAP have been aligned against our PREPL_S structure using the server TM-align (Dong et al., 2018). PREP from *Aeromonas punctata*, PDB ID: 3IUL; AAP from *Aeropyrum pernix*, PDB ID: 3O4G; OpdB from *Trypanosoma brucei*, PDB ID: 4BP8. Note: only residues observed in the structures have been aligned. TM-align outputs the superimposition of the four structures (Figure S4) and the sequence alignment. Totally conserved residues are boxed in red and equivalent residues (residues >70% similar, considering physicochemical properties) are shown in red and boxed in blue. The secondary structure elements of the PREPL and OpdB models are depicted on top and below, respectively. Active site residues (Ser, Asp and His) and PREPL G652, F585, W607 and OpdB E655 are highlighted with green boxes.
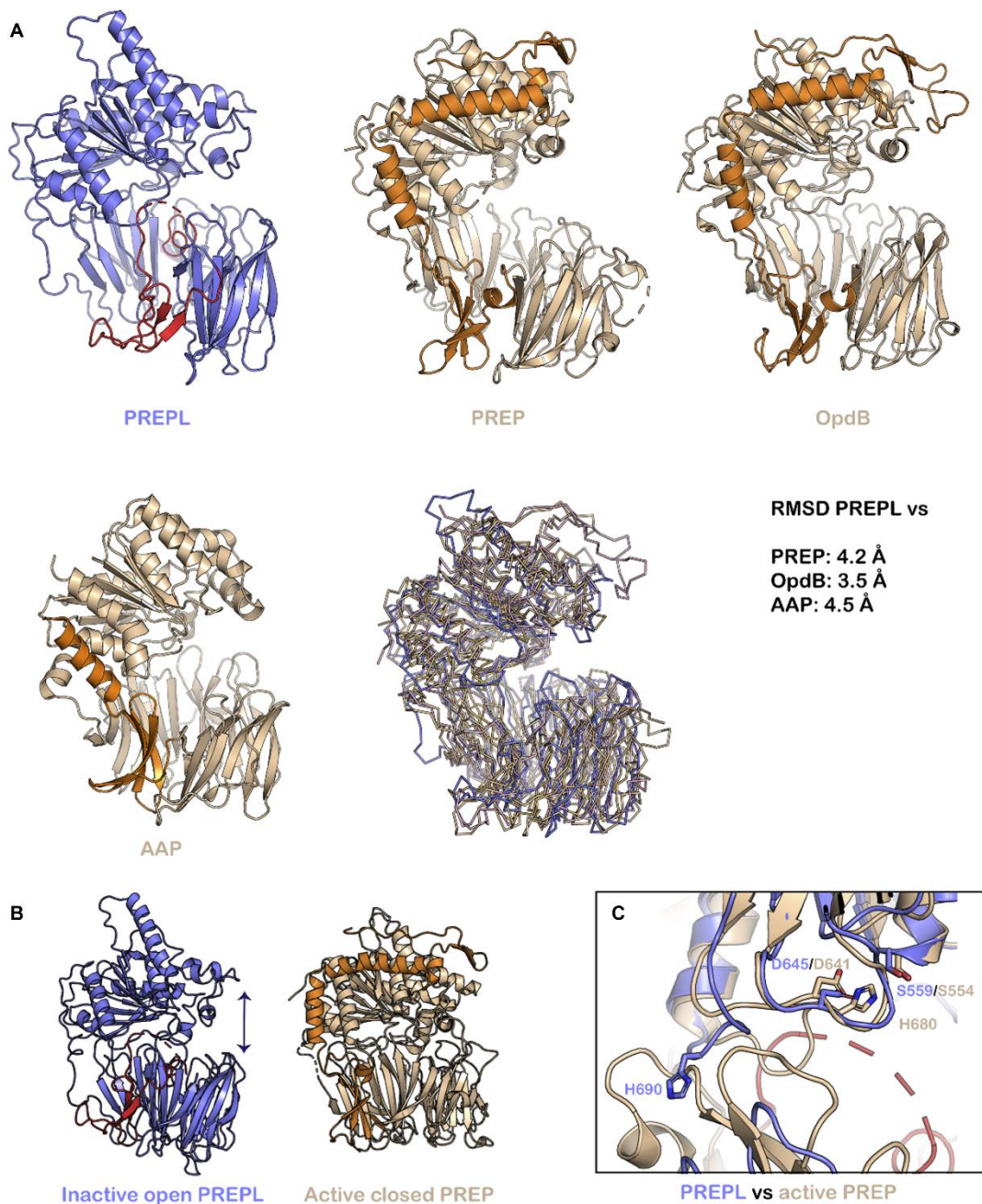
Figure S5. Human PREPLₛ structure is solved in inactive open conformation. Related to Figure 5.

A. Superposition of human PREPLₛ and the open structures of PREP, OpdB and AAP, giving RMSD values of 4.2, 3.5 and 4.5Å, respectively (calculated by TM-align). The amino-terminus and blade-1 are highlighted in red (PREPL) and in orange (PREP, OpdB, AAP). In the overlay, PREPLₛ is shown in blue, PREP in beige, OpdB in pink and AAP in yellow. B.-C. Comparison of human PREPLs (blue with amino-terminus and blade 1 in red) and human PREP (PBD ID 3DDU) (beige with amino-terminus and blade 1 in orange), highlighting the interdomain opening in PREPLs (B) and the ~20Å outward swing of H690 with respect to the active position of H680 (C).
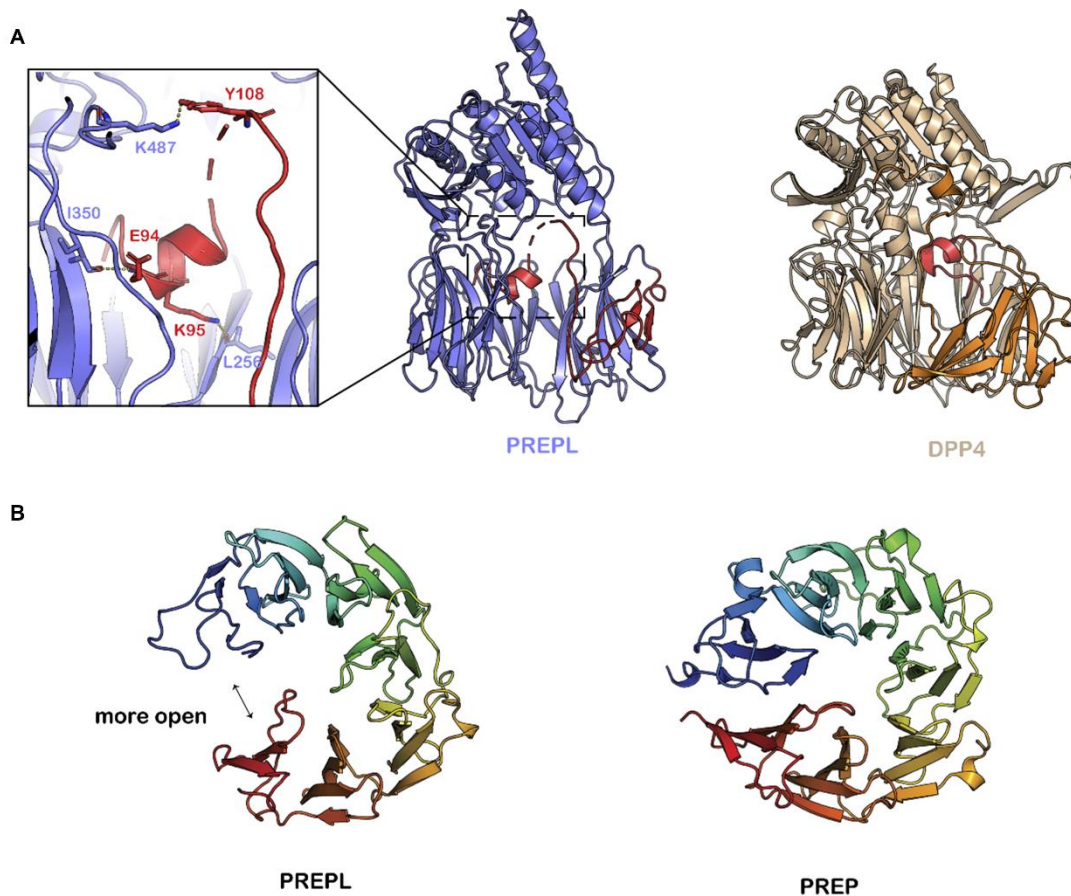
Figure S6. The amino-terminus and the first blade of the β-propeller domain of PREPL$_S$ differ from the peptidase family members. Related to Figure 5.

A. PREPL$_S$ is shown in blue cartoon, with the amino-terminus and blade 1 in red, as in Figure 5. The left panel shows the hydrogen bonds between the amino-terminus and the rest of the protein. The electron density for residues 101-107 is very weak and this region could not be modeled. The amino-terminal helix makes only two direct interactions with the rest of the protein (E94 main chain-I350 main chain and K95 side chain-L256 main chain). The only other contact of the amino-terminus to the rest of the protein is Y108 side chain-K487 side chain. The helix that the amino-terminus forms within the top of the funnel, resembles the helix that can be found in the structure of dipeptidyl peptidase IV (DPP4) (PDB ID 1R9N), shown in the right panel. DPP4 is shown in beige cartoon, with the amino-terminus and blades 1 and 2 in orange and the helix at the center of the funnel highlighted in red. B. The β-propeller domains of PREPL$_S$ and PREP are shown in cartoon, as seen from the bottom of the structure, where the blades of the propeller can be appreciated. In PREPL$_S$, the blades 1 and 7 (in blue and red, respectively) are further apart than in the PREP structure.
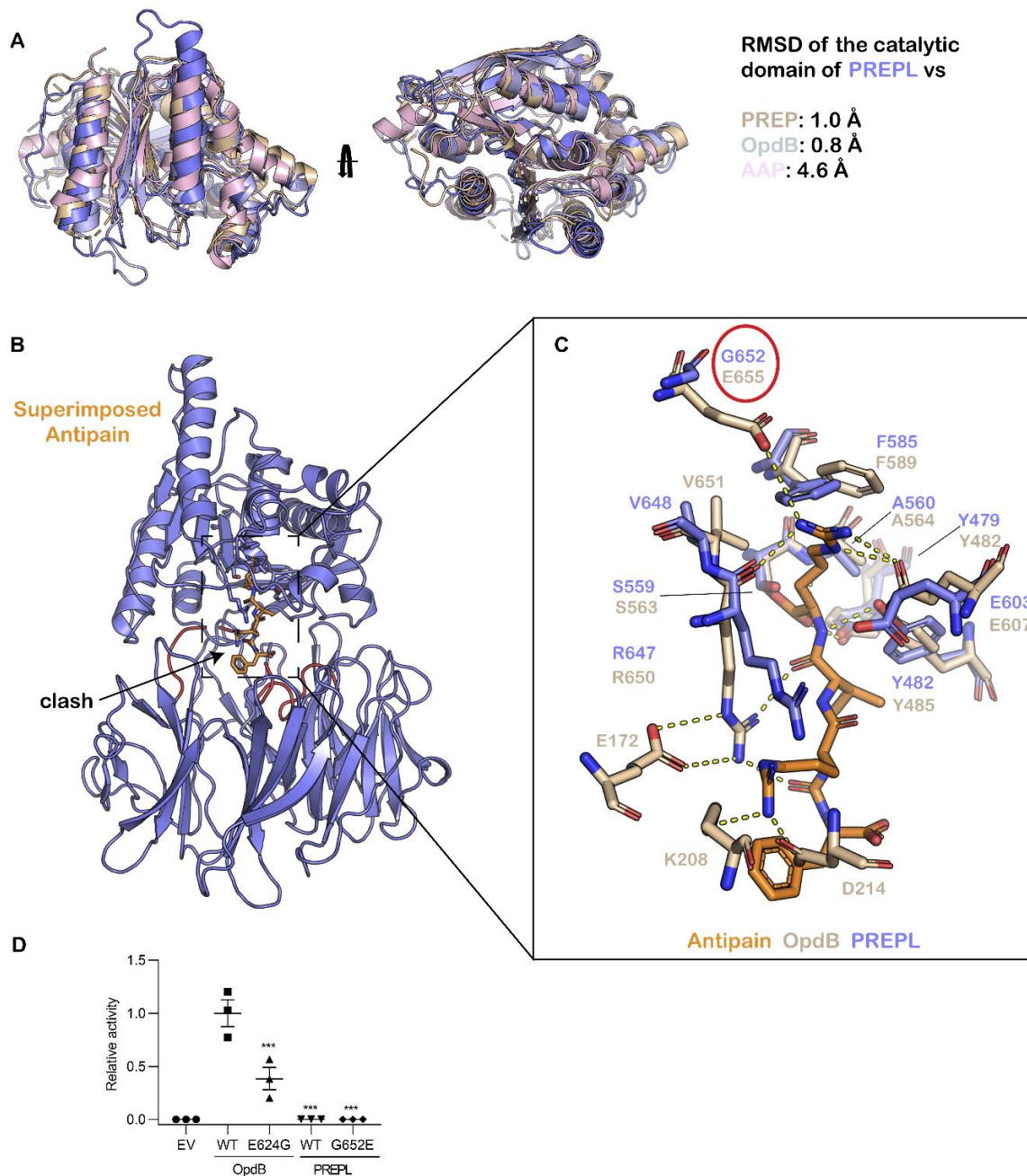
Figure S7. Similar catalytic domain structure in the prolyl oligopeptidase family despite different substrate specificity. Related to Figure 5.
A. Superposition of the catalytic domain of PREPL$_S$ with the catalytic domain of PREP, OpdB and AAP, highlighting the α/β hydrolase fold conservation. B. The OpdB inhibitor Antipain (orange sticks) modeled inside the PREPL$_S$ cavity. The clash between the inhibitor and the amino-terminus (in red) can be observed. C. Detailed view of the peptide-binding pocket of *Trypanosoma brucei* OpdB, PDB ID: 4BP9 (residues in beige sticks) bound to Antipain (orange sticks) (Canning et al., 2013). The PREPL$_S$ structure is superimposed (blue sticks), showing how all residues are conserved, except E655 (G652 in PREPL$_S$). Equivalent residues to those belonging to the β-propeller domain (E172, K208 and D214) cannot be predicted as we have the PREPL$_S$ open structure. D. Peptidase activity assay showing the 2-fold loss of activity of the *E. coli* OpdB E624G mutant while the PREPL$_S$ G652E mutant does not gain peptidase activity. z-Arg-Arg-AMC was used as substrate. Data shown as mean ± SEM (n=3), one-way ANOVA with Dunnett's multiple comparison test.

Table S1. Protein interaction partners of PREPL identified by MAPPIT and listed in BIOGRID. Related to Figure 2.

The interactors of PREPL were determined by MAPPIT. Each specific bait-prey interaction was studied in parallel with two controls (irrelevant bait (IB) and irrelevant prey (IP)). The fold change of the specific bait-prey interaction (stimulated/nonstimulated) should be higher than the fold change of the control samples.

pSEL(+2L)-PREPL interactors

Entrez_ID	Min. of BP/PIB and BP/BIP	Entrez_ID	Min. of BP/PIB and BP/BIP	Entrez_ID	Min. of BP/PIB and BP/BIP
PLEKHO2	217,4	SSX5	23,7	PSMA1	10,3
BEX1	181,9	SCT	23,2	DLEU7	10
INGX	177,7	RASL12	23,1	CLASP1	9,9
DISC1	165	TRAPPC1	23	BET1L	9,6
C2orf48	139,4	C22orf32	22	GMFG	9,4
PIN4	136,1	FLJ46257	21,5	AKR1C1	9,2
ADM2	101,1	DCTN5	21,1	UPP1	9,2
CAMK2G	99,3	CN5H6.4	20,8	MTFMT	9,2
NRIP3	98,2	DYX1C1	20,7	CRYBB3	8,8
BPY2	90,6	MGC39545	20,6	C9orf46	8,8
BOLA3	80,5	FAM98A	20,5	EDIL3	8,6
BEX4	70,6	PSMG2	20,5	TTI1	8,6
BEX2	69,5	GRB7	20,4	PGAM4	8,5
RFT1	68,6	LOC1001295	20,4	SPSB2	8,4
CDH23	68	RAPGEF6	19,9	PCGF5	8,4
DNAJC10	66,8	C5orf20	19,2	HRASLS2	7,7
TCF15	65,8	EIF4E2	19	PHYH	7,5
SSX4	62,8	NUDT6	18,9	CCDC96	7,3
LOC284276	59,7	SH2D2A	18,3	VGLL1	7,2
LOC285033	57,3	SIRT6	18,3	C11orf40	7,1
MDM1	57,1	LDHAL6A	18,2	DTX3L	6,8
PNRC2	56,4	GRAP2	18,2	SNX4	6,7
PDK1	55	LACTB	18,2	SMOC1	6,6
UBL5	53,8	MAP4	17,2	CUL3	6,6
ARPC5L	52,2	NIPSNAP3B	17,1	C19orf54	6,2
ATG4C	48,9	IGLV2-14	17	FAM215A	6,1
SSH3	46,2	TCAP	16,7	CSNK1D	6,1
GRXCR1	46	SUOX	16,7	SNRK	6
SF3B14	45,7	ATP5I	16,6	NDUFS3	6
LDOC1L	45,1	SH3RF2	16,2	C2orf65	5,7
MRPL11	42	POLL	16,1	RDH13	5,6
MTHFD2	41,7	CLLU1	16,1	C16orf80	5,5
TCAP	41,6	PHKG2	16	CCDC130	5,5
SORD	37,8	KIF19	15,9	ANKRD55	5,2
MRPS12	36,9	SETD9	15,8	ASPSCR1	5
ECHDC1	34,5	TESPA1	15,6	MRPS23	4,8
ARL2	34,4	RAB15	15,5	AIFM2	4,7
COMMD4	34,3	CYLC2	14,5	LGALS13	4,6
NDUFV2	34,2	STK38	13,3	LARS	4,5
LOC401431	34,1	PSMB1	13,2	MTERFD3	4,4
C18orf54	32,9	SAMD12	13,2	AKR7A3	4,3
FMO5	30,9	VPS53	13	HELLS	4,2
FAM167B	29,9	CCNG2	12,7	IL17D	3,9
NFKBID	29,2	SPANXN3	12,4	DACT2	3,8
STX5	29,2	ERC1	12,3	PPP3CA	3,7
TRIM41	29,1	TAGAP	12,2	C10orf85	3,6
SSX6	29,1	NTAN1	12,1	STAU2	3,4
THAP11	28,6	RPS15A	12	FKBP9	3,4
SPAG11B	28,1	MRPL46	12		
MRRF	28	RELA	11,8		
NT5C3	27,9	MSRA	11,5		
SCO2	27,4	TCL1B	11,5		
NDUFS4	26,6	SYT11	11,2		
NDFIP2	26,5	EIF2C3	10,9		
RAB40AL	25,9	HSD17B8	10,8		
MRPL53	25,9	CBR4	10,8		
LOC142937	25,1	RASL11A	10,7		
PRDM5	24,8	CCDC42	10,6		
CARD16	24,3	GAST	10,6		
PSD3	24,2	SSX7	10,6		

pCLG20-PREPL interactors

Entrez_ID	Min. of BP/PIB and BP/BIP
ZBTB44	529,7
AIFM1	386,5
IDE	345,7
SPICE1	340,5
FRMD1	260,9
MRPL28	255,1
METTL22	247,5
CCRN4L	221,4
CDK16	211,1
LOC149134	209,6
MRPL12	208,4
POLR3D	204,9
MZT1	203,8
RGS4	201,7
MCEE	189,3
CEP41	184,6
RAD51AP1	177,5
MRPS24	169,8
SEPSECS	162,2
MRPS2	162
CKMT2	151,1
C4orf17	144,2
FNDC8	136,9
COL9A1	136,5
NDNL2	133,4
GRB10	127,7
KRT7	120,7
C12orf74	118,1
DAPP1	111,8
C21orf88	110,8
C17orf102	108,6
POLR2E	103,9
HUNK	102,2
POP7	96,4
SSBP1	94,9
GTSF1L	94,1
ECH1	92,7
MTMR10	87,3
ENSA	86,9
MMAB	83,7
SOCS7	82,9
RBM4	81,5
APBB2	76,2
ABT1	73,2
HDC	70,2
CLPP	70,1
CAMK1G	65,2
NAA11	64,3
ABRA	61
CKMT1B	60,4
PDZD7	60,2
FAM110B	58,8
COX5B	52,5
ACAP3	51,2
HSPA12B	47
SHC4	46,9
HDAC11	44,4
PLK1S1	43,6
ANGPTL4	41,3
GTPBP5	39,9
PIF1	38,5
CDK5R1	35,8
MICU3	35,5
ECH1	35,2
TBC1D20	34,5
CCDC8	32,5
VAV3	32,2
C6orf141	26,2
TSKS	24,9

Entrez_ID	Min. of BP/PIB and BP/BIP
KRT79	24,9
PRR25	17,6
SRMS	17,2
KCTD13	16,9
STAC3	14,9
C1orf229	14,5
GNG8	13,9
SF3A2	13,4
ZADH2	10,6
FRAT2	9,9
TBC1D3B	9,5
PABPN1L	6,5
DMGDH	5,1
C20orf132	4,1
ECSIT	3,8

BIOGRID: PREPL interactors

* Interactors also identified in MAPPIT

Protein	Reference
COIL	Lim (2006)
ELAVL1	Abdelmohsen (2009)
USP22	Sowa (2009)
APEH	Havugimana (2012)
FTSJ2/MRM2	Huttlin (2014)
MRPS25	Huttlin (2014)
TEX30	Huttlin (2014)
SLIRP	Huttlin (2014)
CBR4 *	Huttlin (2014)
METTL2A	Huttlin (2014)
ADCK3/COQ8/	Huttlin (2014)
UQCRFS1	Huttlin (2014)
TUFM	Huttlin (2014)
CRYZ	Huttlin (2014)
LIG3	Huttlin (2015)
ACAA2	Huttlin (2015)
UNKL	Huttlin (2015)
RARS2	Huttlin (2015)
TTC39B	Huttlin (2015)
GOT2	Floyd (2016)
PREPL	Floyd (2016)
PMPCA	Floyd (2016)
C1QBP	Floyd (2016)
MRPL10	Huttlin (2017)
RGS4 *	Huttlin (2017)
PDHX	Huttlin (2017)
MRPS34	Huttlin (2017)
SDHB	Huttlin (2017)
MRPL41	Huttlin (2017)
ARHGAP36	Huttlin (2017)
PDDC1	Huttlin (2017)
C4ORF26	Huttlin (2017)
YBEY	Huttlin (2017)
MRM1	Liu (2018)
HSPD1	Liu (2018)
PDK1 *	Liu (2018)
TRMT61B	Liu (2018)

Table S2. Protein interaction partners of PREPL linked to mitochondrial function. Related to Figure 2.

MITOCHONDRIA	Entrez_ID	Protein
g:profiler: GO:CC - *GO:ID 0005739*	ACAA2	Acetyl-CoA Acyltransferase 2
	AIFM1	apoptosis inducing factor mitochondria associated 1
	AIFM2	apoptosis inducing factor, mitochondria associated 2
	ARL2	ADP ribosylation factor like GTPase 2
	ATP5I/ATP5ME	ATP synthase membrane subunit E
	BOLA3	bolA family member 3
	C1QBP	Complement C1q Binding Protein
	CBR4	carbonyl reductase 4
	CKMT1B	creatine kinase, mitochondrial 1B
	CKMT2	creatine kinase, mitochondrial 2
	CLPP	caseinolytic mitochondrial matrix peptidase proteolytic subunit
	ADCK3/COQ8A	Coenzyme Q8A
	COX5B	cytochrome c oxidase subunit 5B
	DISC1	disrupted in schizophrenia 1
	DMGDH	dimethylglycine dehydrogenase
	ECH1	enoyl-CoA hydratase 1
	ECSIT	ECSIT signalling integrator
	FAM110B	family with sequence similarity 110 member B
	GOT2	Glutamic-Oxaloacetic Transaminase 2
	HSD17B8	hydroxysteroid 17-beta dehydrogenase 8
	HSPD1	Heat Shock Protein Family D (Hsp60) Member 1
	IDE	insulin degrading enzyme
	LACTB	lactamase beta
	LIG3	DNA ligase 3
	MCEE	methylmalonyl-CoA epimerase
	MICU3	mitochondrial calcium uptake family member 3
	MMAB	methylmalonic aciduria (cobalamin deficiency) cblB type
	MRM1	Mitochondrial RRNA Methyltransferase 1
	FTSJ2/MRM2	Mitochondrial RRNA Methyltransferase 2
	MRPL10	Mitochondrial Ribosomal Protein L10
	MRPL11	mitochondrial ribosomal protein L11
	MRPL12	mitochondrial ribosomal protein L12
	MRPL28	mitochondrial ribosomal protein L28
	MRPL41	Mitochondrial Ribosomal Protein L41
	MRPL46	mitochondrial ribosomal protein L46
	MRPL53	mitochondrial ribosomal protein L53
	MRPS12	mitochondrial ribosomal protein S12
	MRPS2	mitochondrial ribosomal protein S2
	MRPS23	mitochondrial ribosomal protein S23
	MRPS24	mitochondrial ribosomal protein S24
	MRPS25	Mitochondrial Ribosomal Protein S25
	MRPS34	Mitochondrial Ribosomal Protein S34
	MRRF	mitochondrial ribosome recycling factor
	MSRA	methionine sulfoxide reductase A

MTERFD3	mitochondrial transcription termination factor 2	
MTFMT	mitochondrial methionyl-tRNA formyltransferase	
MTG2	mitochondrial ribosome associated GTPase2	
MTHFD2	methylenetetrahydrofolate dehydrogenase (NADP+ dependent) 2, methenyltetrahydrofolate cyclohydrolase	
NDFIP2	Nedd4 family interacting protein 2	
NDUFS3	NADH:ubiquinone oxidoreductase core subunit S3	
NDUFS4	NADH:ubiquinone oxidoreductase subunit S4	
NDUFV2	NADH:ubiquinone oxidoreductase core subunit V2	
NIPSNAP3B	nipsnap homolog 3B	
CCRN4L/NOCT	nocturnin	
NUDT6	nudix hydrolase 6	
PDHX	Pyruvate Dehydrogenase Complex Component X	
PDK1	pyruvate dehydrogenase kinase 1	
PHYH	phytanoyl-CoA 2-hydroxylase	
PIF1	PIF1 5'-to-3' DNA helicase	
PIN4	peptidylprolyl cis/trans isomerase, NIMA-interacting 4	
PMPCA	Peptidase, Mitochondrial Processing Alpha Subunit	
PPP3CA	protein phosphatase 3 catalytic subunit alpha	
RAB40AL	RAB40A, member RAS oncogene family-like	
RARS2	Arginyl-TRNA Synthetase 2, Mitochondrial	
RDH13	retinol dehydrogenase 13	
SCO2	SCO2, cytochrome c oxidase assembly protein	
SDHB	Succinate Dehydrogenase Complex Iron Sulfur Subunit B	
SLIRP	SRA Stem-Loop Interacting RNA Binding Protein	
C22orf32/SMDT1	Single-Pass membrane protein with aspartate rich tail 1	
SORD	sorbitol dehydrogenase	
SSBP1	single stranded DNA binding protein 1	
SUOX	sulfite oxidase	
TRMT61B	TRNA Methyltransferase 61B	
TUFM	Tu Translation Elongation Factor, Mitochondrial	
UQCRFS1	Ubiquinol-Cytochrome C Reductase, Rieske Iron-Sulfur Polypeptide 1	

MITOCHONDRIAL TRANSLATION *g:profiler: GO:BP - GO:ID 0032543*	Entrez_ID	Protein
	C1QBP	Complement C1q Binding Protein
	MRPL10	Mitochondrial Ribosomal Protein L10
	MRPL11	mitochondrial ribosomal protein L11
	MRPL12	mitochondrial ribosomal protein L12
	MRPL28	mitochondrial ribosomal protein L28
	MRPL41	Mitochondrial Ribosomal Protein L41
	MRPL46	mitochondrial ribosomal protein L46
	MRPL53	mitochondrial ribosomal protein L53
	MRPS12	mitochondrial ribosomal protein S12
	MRPS2	mitochondrial ribosomal protein S2
	MRPS23	mitochondrial ribosomal protein S23
	MRPS24	mitochondrial ribosomal protein S24
	MRPS25	Mitochondrial Ribosomal Protein S25

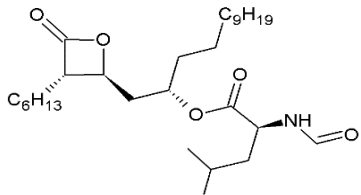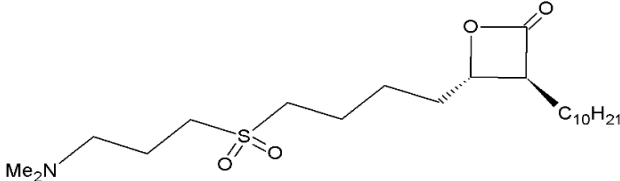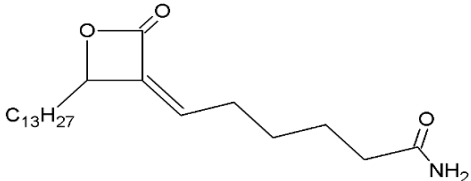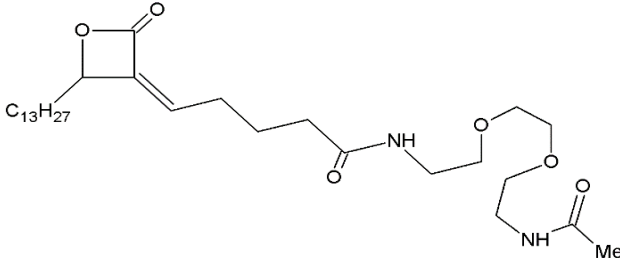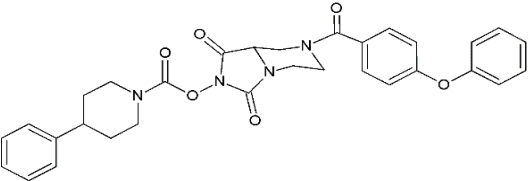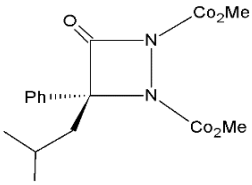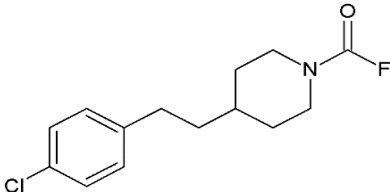| | MRPS34 | Mitochondrial Ribosomal Protein S34 |
	MRRF	mitochondrial ribosome recycling factor
	MTG2	mitochondrial ribosome associated GTPase2
	RARS2	Arginyl-TRNA Synthetase 2, Mitochondrial
	TUFM	Tu Translation Elongation Factor, Mitochondrial
OXPHOS	Entrez_ID	Protein
	ATP5I/ATP5ME	ATP synthase, H+ transporting, mitochondrial Fo complex subunit E
	COX5B	cytochrome c oxidase subunit 5B
	ECSIT	ECSIT signalling integrator
	NDUFS3	NADH:ubiquinone oxidoreductase core subunit S3
	NDUFS4	NADH:ubiquinone oxidoreductase subunit S4
	NDUFV2	NADH:ubiquinone oxidoreductase core subunit V2
	SCO2	SCO2, cytochrome c oxidase assembly protein
	SDHB	Succinate Dehydrogenase Complex Iron Sulfur Subunit B
	UQCRFS1	Ubiquinol-Cytochrome C Reductase, Rieske Iron-Sulfur Polypeptide 1
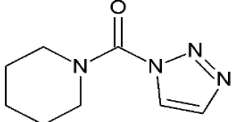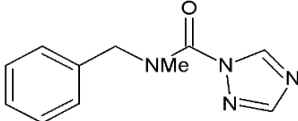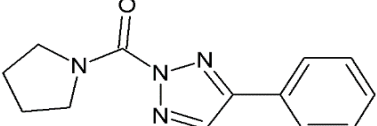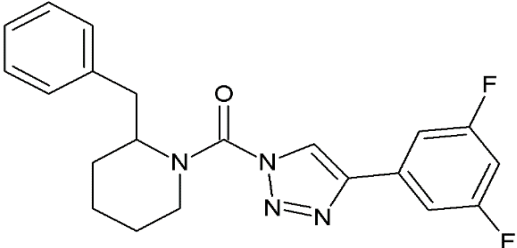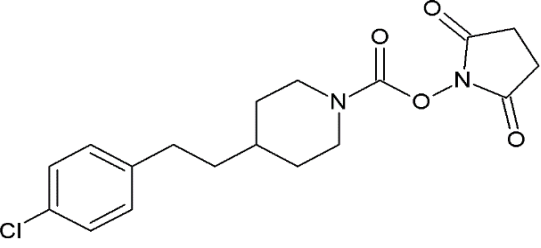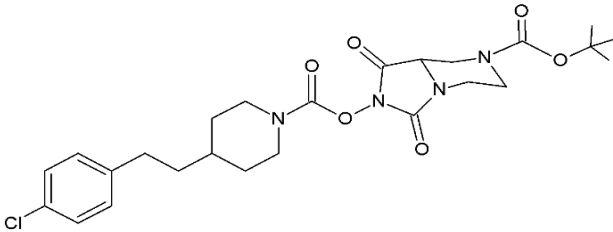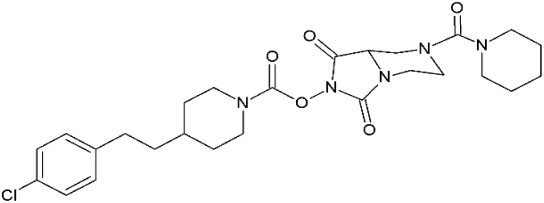
Table S3. *In silico* prediction analysis of mitochondrial targeting signal in PREPL. Related to Figure 2.

	MitoFates	TargetP-2.0	iPSORT	MitoProtII
hPREPL$_L$	0.131	0.1288	No	No
hPREPL$_S$	0.000	0	No	No
mPREPL$_L$	0.845	0.8198	Yes	Yes
mPREPL$_S$	0.000	0.0001	No	No

Table S4. Serine hydrolase inhibitor library used in competitive ABPP. Related to Figure 4.

Number (blot)	Compound name	Chemical structure
A1	Tetrahydrolipstatin	
A2	Palmostatin M	
A3	KC01	
A4	WHP-III-44-DEG	
B1	AA-26-9	
B2	JMN203	
B3	AA-32-1	

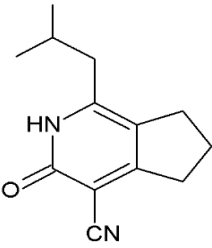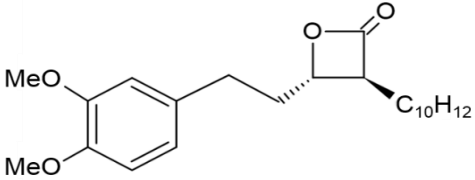|		
B4	KLH41	
C1	MJN-2013-9	
C2	JJH221	
C3	JJH250	
C4	JJH309	
D1	ABL113	
D2	WHP313	

Inhibitor 8	1-isobutyl-3-oxo-3,5,6,7-tetrahydro-2H-cyclopenta[c]pyridine-4-carbonitrile	
PalmB	Palmostatin B	

Table S5. Data collection and refinement statistics for PREPL. Related to Figure 5.

	PREPL
Data collection	
Wavelength (Å)	0.9794
Resolution range (Å)	44.53 - 3.1 (3.211 - 3.1)
Space group	I222
Unit cell dimensions	
a, b, c (Å)	64.92, 150.88, 220.66
α, β, γ (°)	90, 90, 90
Total reflections	148699 (14533)
Unique reflections	37881 (3777)
Multiplicity	3.9 (3.9)
Completeness (%)	99.87 (99.66)
$I/\sigma(I)$	11.72 (1.03)
Wilson B-factor (Å²)	104.69
R_{merge} (%)	0.09381 (1.22)
R_{meas} (%)	0.1088 (1.419)
$R_{p.i.m}$ (%)	0.0548 (0.7159)
CC1/2	0.998 (0.488)
CC*	0.999 (0.81)
Refinement	
Reflections used in refinement	37970 (3768)
Reflections used for R-free	1925 (168)
R_{work} (%)	0.2450 (0.5063)
R_{free} (%)	0.2821 (0.5616)
CC_{work}	0.934 (0.583)
CC_{free}	0.942 (0.249)
Number of non-hydrogen atoms	5021
Macromolecules	5021
Ligands	0
Solvent	0
Protein residues	624
RMSD, bonds (Å)	0.002
RMSD, angles (°)	0.59
Ramachandran favored (%)	89.84
Ramachandran allowed (%)	10.16
Ramachandran outliers (%)	0.00
Rotamer outliers (%)	0.36
Clashscore	9.15
Average B-factor (Å²)	125.89
Macromolecules	125.89
Number of TLS groups	2

Statistics for the highest-resolution shell are shown in parentheses.

Table S6. Primers used for RT-qPCR, genotyping and MAPPIT cloning (listed in 5'-3' direction). Related to Methods.

RT-qPCR

Gene	Forward primer	Reverse primer
mβactin	AGCCATGTACGTAGCCATCC	TCTCAGCTGTGGTGGTGAAG
mNdufs3	TGTCTCTGCGGTTCAACTCT	GGATGTCCCTCGAAGCCATA
mNd1	TGCACCTACCCTATCACTC	ATTGTTTGGGCTACGGCTC
mSdha	ATTTGGTGGACAGAGCCTCA	GGCACTCCCCATTTTCCATC
mUqcrc1	TTGCCCAGAAACACTTGAGC	GTCACGTTGTCTGGGTTAGC
mCytb	TACCTGCCCCATCCAACATT	TAAGCCTCGTCCGACATGAA
mCoxIV	CCATGTCACGATGCTGTCTG	CTCCCAAATCAGAACGAGCG
mCo1	ACCCAGATGCTTACACCACA	TGTGATATGGTGGAGGGCAG
mAtp5	GTACTCCGCTCTGATCATCG	CTCTTCTTTTCCTCCGCTGC
mAtp6	CCACACACCAAAAGGACGAA	GAAGGAAGTGGGCAAGTGAG

Mouse genotyping

Primer name	Forward primer	Reverse primer
Δ	TCTTGCTGTTCCTCCTAGCC	GTCCTGACAAACGGAAAAGG
LoxP	GGCAGCTGTAGGAAGTCAGC	ATGTCACAGGCTCGTGTTTG

MAPPIT

Primer name	Forward primer	Reverse primer
pSEL(+2L)	GCCAGCGTCGACCATGGATGCATTTG	CGAGTTGCGGC CGCTCAGAATTTCAG
pCLG20	GCCAGCGAGCTCCATGGATGCATTTG	CGAGCTTGGGCCCTCAGAATTTCAGG